Work at JMA on Ensemble Forecast Methods

**Hitoshi Sato[1], Shuhei Maeda[1], Akira Ito[1],
Masayuki Kyouda[1], Munehiko Yamaguchi[1], Ryota Sakai[1],
Yoshimitsu Chikamoto[2], Hitoshi Mukougawa[3] and Takuji Kubota[4]**

[1]*Japan Meteorological Agency, Tokyo, Japan*
[2]*Center for Climate System Research, University of Tokyo, Kashiwa, Japan*
[3]*Disaster Prevention Research Institute, Kyoto University, Kyoto, Japan*
[4]*Earth Observation Research Center, Japan Aerospace Exploration Agency, Tsukuba, Japan*

1 Introduction

The tropical intraseasonal oscillation (ISO), known as the Madden-Julian Oscillation (Madden and Julian, 1994), is the most dominant component in the tropical intraseasonal variability in the troposphere. The variation in convective activity associated with the tropical ISO accompanies the characteristic large-scale circulation anomaly, affecting the extratropical medium and extended range weather forecasts (Waliser et al., 2003; Jones et al.,2004). Kubota et al. (2005) indicated that initial perturbations produced by a Breeding of Growing Modes (BGM) method (Toth and Kalnay, 1993, 1997) in the operational medium-range and monthly ensemble prediction system (EPS) of the Japan Meteorological Agency (JMA) are characterized by extratropical baroclinic unstable modes. In addition, kinetic energy of these initial perturbations in the tropical regions is too large for predicting the tropical atmospheric circulation. This is because the norm of the initial perturbations in the operational BGM method of the JMA system is defined by the 500-hPa geopotential height variance. Thus, we modify the BGM method to create initial perturbations that are adequate to predict the tropical ISO (Chikamoto et al., 2007). The modification of the BGM method and obtained tropical bred vectors are shown in Section 2 and 3. In the monthly EPS, it is more important to predict the tropical ISO and to estimate uncertainties associated with the tropical ISO than in the medium-range EPS. Therefore, these perturbations have been introduced in the operational monthly EPS in March 2007.

On the other hand, JMA has upgraded the medium-range EPS in November 2007 (Table 1). The major updates are to change the generator to a singular vector (SV) method and to increase the resolution of the EPS model to TL319L60. JMA also has a plan to introduce the typhoon EPS with SVs in 2008. The JMA SV method and its characteristics are shown in Section 4 and 5. A conclusion is given in Section 6.

2 Modification of the BGM Method in the JMA monthly EPS

In the operational JMA monthly EPS, the initial perturbations are obtained by the BGM method as follows. At first, the model is integrated for 12 hours from the 24 perturbed and the unperturbed initial conditions. The differences between the unperturbed control and each of the perturbed 12 hour forecasts are normalized, i.e., rescaled every 12 hours using a specified norm of the perturbation. And each perturbation is orthonormalized every 24 hours. The norm is defined by using area-averaged root-mean square (RMS) variations of the 500-hPa geopotential height (Z_{500}) north of 20°N. The magnitude of the norm is set to be 14.5% of the climatological RMS Z_{500} variations. The perturbations are added to (or subtracted from) the analysis to create the next set of perturbations. The resulting set of orthonormal perturbations is mathematically related to the local Lyapunov vectors, and referred to as bred vectors. As Toth and Kalnay (1997) indicated, the spatial structure of the obtained leading bred vector is well characterized by baroclinic unstable modes since these modes have the

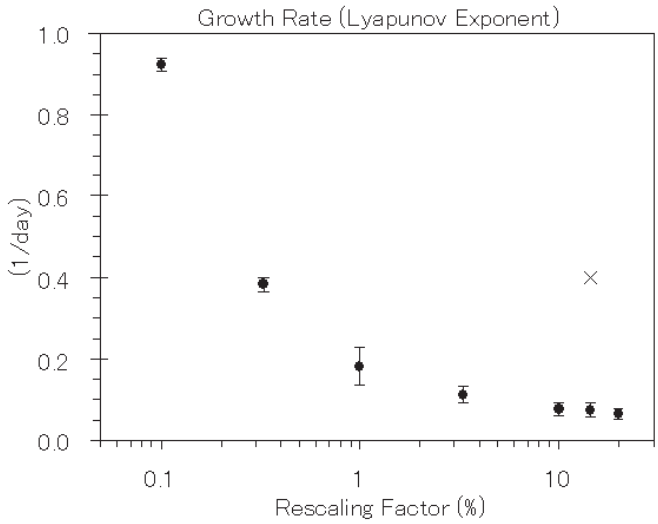

Figure 1: The time-mean growth rate of the leading tropical bred vector for a 92-day period with rescaling factors of 0.1%, 0.33%, 1%, 3.3%, 10%, 14.5%, and 20% of the climatological RMS variance of the 200-hPa velocity potential. Closed circles (cross) indicate the time-mean growth rate of tropical (extratropical) bred vectors. Each error bar is estimated from the standard deviation of the time-mean growth rate for a 30-day period.

largest growth rate in large-scale atmospheric motions. Thus, the operational breeding cycle of JMA is adequate to obtain growing errors in the extratropics associated with the baroclinic instability.

In the tropical region, however, the amplitude of 200-hPa velocity potential (χ_{200}) of the bred vector of the JMA ensemble prediction system tends to be too large to predict tropical atmospheric circulations (Kubota et al., 2005). Therefore, we have modified the operational breeding cycle of JMA to obtain suitable initial perturbations in the tropical region. First, the norm of the perturbation is defined by an area-averaged RMS χ_{200} variation in the tropical belt from 20°S to 20°N. Second, the magnitude of variables (X) associated with initial perturbation of the breeding cycle is exponentially damped in the extratropics poleward of 20°S and 20°N as follows:

$$\begin{cases} X & \text{for } |\phi| \leq 20^\circ \\ X \exp\{-(|\phi| - 20^\circ)^2/50\} & \text{for } |\phi| > 20^\circ \end{cases} \quad (1)$$

where ϕ is latitude. Since these tapered perturbations would effectively reduce the vigorous baroclinic instability prevailing in the extratropics, we obtain perturbations related to the tropical atmospheric circulation. Third, each perturbation is normalized, i.e., rescaled every 24 hours but not orthogonalized, which is intended to check the existence of a growing unstable mode in the tropical regions. The magnitude of the norm is set to be 20%, 14.5%, 10%, 3.3%, 1%, 0.33%, and 0.1% of the climatological RMS χ_{200} variance. This is done in different breeding cycle runs in order to test the sensitivity of the bred vector with respect to the amplitude. We start the modified breeding cycles from 15 October 2003 for two random perturbations, and obtain two bred vectors for each magnitude of the norm. Although results only for the leading bred vector will be shown in the following section, the second bred vector has similar dynamical properties to the leading bred vector. The similarity between these two bred vectors also suggests the existence of an unstable mode. The analysis on the bred vectors was made during a period from 1 November 2003 to 31 January 2004 when active tropical ISO was observed.

3 Tropical Bred Vectors

First of all, we examined the dependence of dynamical properties of the bred vector on the magnitude of the norm, i.e., the rescaling factor. Figure 1 shows the relationship between the rescaling factor and the time-mean

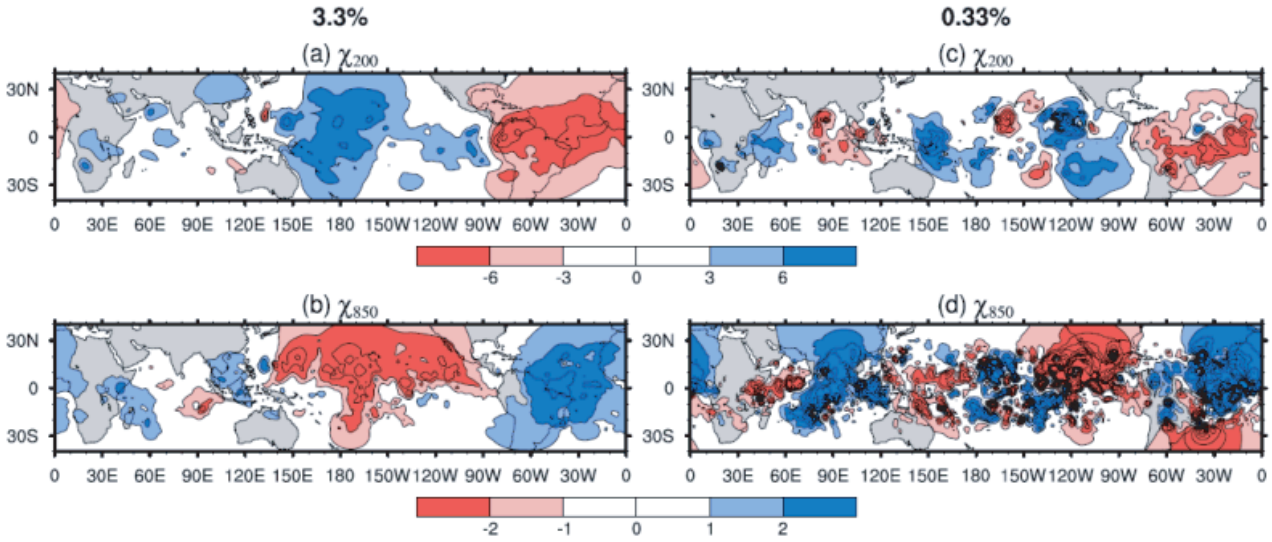

Figure 2: Snapshots of (a,c) 200-hPa and (b,d) 850-hPa velocity potential fields of tropical bred vectors on 26 November 2003. The left (right) plots show tropical bred vectors with rescaling factor of 3.3% (0.33%) of the climatological RMS variance of 200-hPa velocity potential. Amplitudes of these bred vectors are normalized. Positive (negative) values indicate convergence (divergence). The contour intervals are $3 \times 10^5 \mathrm{m}^2\ \mathrm{s}^{-1}$ *at top plots and* $1 \times 10^5 \mathrm{m}^2\ \mathrm{s}^{-1}$ *at lower plots.*

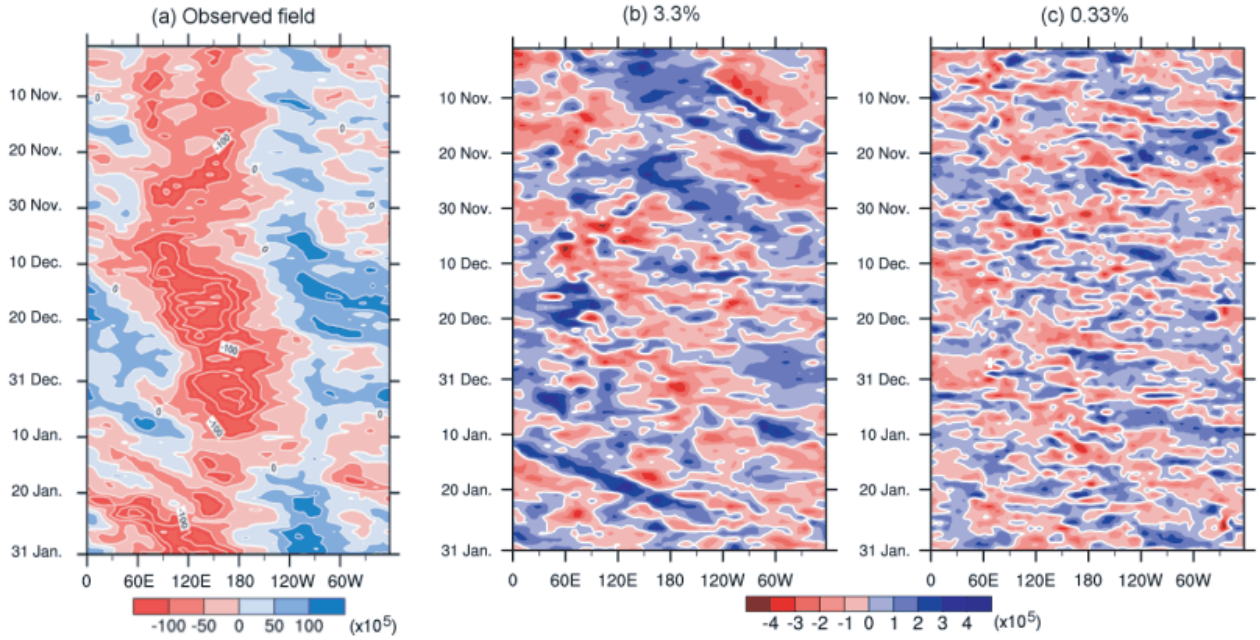

Figure 3: Hovmöller diagrams of 200-hPa velocity potential averaged over the $10^\circ S$-$10^\circ N$ *region for (a) the observed field, (b) the bred vector for a rescaling factor of 3.3%, and (c) the bred vector for a rescaling factor of 0.33%. Amplitudes of these bred vectors are normalized. The contour interval at the left plot (center and right plots) is* $50 \times 10^5 \mathrm{m}^2\ \mathrm{s}^{-1}$ *(*$1 \times 10^5 \mathrm{m}^2\ \mathrm{s}^{-1}$*). Positive (negative) values indicate convergence (divergence).*

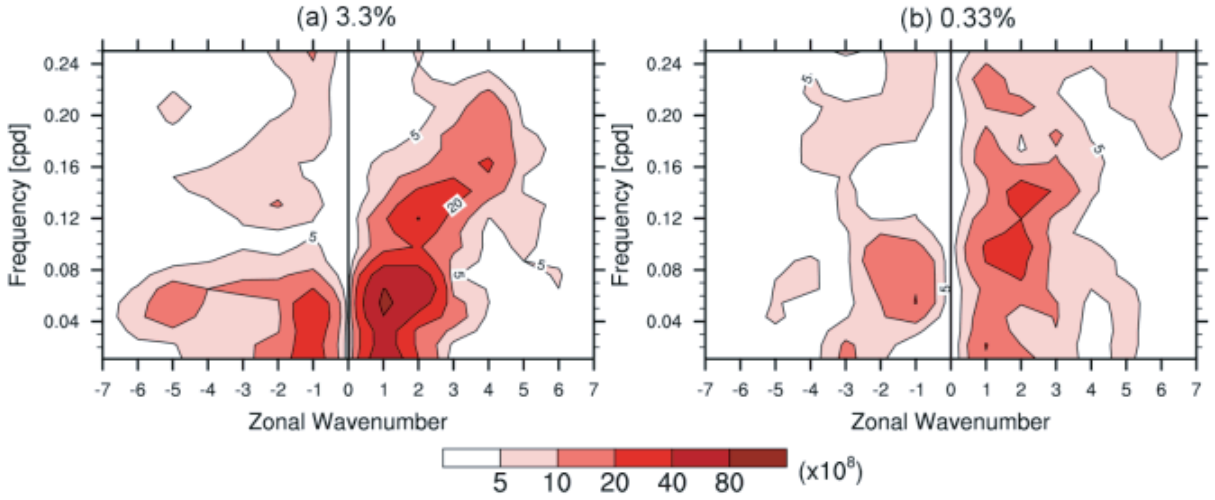

Figure 4: The space-time spectrum of the 200-hPa velocity potential of the tropical bred vector averaged over the 10°S-10°N region. The spectral power is smoothed with a 1-3-5-3-1 filter in frequency. The horizontal and vertical axes are zonal wave number and frequency (cycle per day), respectively. Positive (negative) zonal wave numbers indicate eastward (westward) propagation.

growth rate of the leading tropical bred vector $\mathbf{v}_1(t)$ for the period from 1 November 2003 to 31 January 2004. The leading bred vector $\mathbf{v}_1(t)$ is evaluated every 24 hours, i.e., $t = k\Delta t$ where $k = 1,2,3,\cdots,N$ and $\Delta t = 1$ day. For the analysis period, $k = 1 (k = N = 92)$ corresponds to 1 November 2003 (31 January 2004). The time-mean growth rate $\overline{\alpha}^{N\Delta t}$ during a period of $N\Delta t$ is defined by the following time average of a local in time growth rate $\alpha(k\Delta t)$ for 24 hours:

$$\overline{\alpha}^{N\Delta t} = \frac{1}{N}\sum_{k=1}^{N}\alpha(k\Delta t), \tag{2}$$

$$\alpha(k\Delta t) \equiv \frac{1}{\Delta t}\ln\frac{\|\mathbf{v}_1'((k+1)\Delta t)\|}{\|\mathbf{v}_1(k\Delta t)\|}. \tag{3}$$

Here, $\mathbf{v}_1(k\Delta t)$ is the normalized (rescaled) leading bred vector at $t = k\Delta t$, $\mathbf{v}_1'((k+1)\Delta t)$ the evolved bred vector at $t = (k+1)\Delta t$, and $\|\ \ \|$ the norm of a vector defined by the χ_{200} RMS variance within 20°S-20°N latitude belt. If we take the time-averaging period N in equation (2) to be infinite, and the time evolution of the perturbation is described by a set of linearized equations for the system, then $\overline{\alpha}^{N\Delta t}$ is independent of Δt and equal to the largest Lyapunov exponent. Bred vectors are equal to Lyapunov vectors in the limit of small amplitudes.

The abscissa of Figure 1 denotes the magnitude of $\|\mathbf{v}_1(k\Delta t)\|$ of the climatological RMS χ_{200} variance. Each error bar in Figure 1 indicates the standard deviation of $\overline{\alpha}^{N'\Delta t}$ for $N' = 30$ days, which is computed using all consecutive segments of 30 days from 1 November 2003 to 31 January 2004. When the rescaling factor is 3.3% of the climatological RMS χ_{200} variance, $\overline{\alpha}^{N\Delta t}$ of the leading bred vector has a positive value around 0.1 day^{-1}, corresponding to a doubling time of 7 days. This fact suggests the existence of a dynamically unstable mode associated with large-scale tropospheric motions although the growth rate of the tropical bred vector is considerably smaller than that of the extratropical bred vector. The growth rate of extratropical perturbations dominated by baroclinic unstable modes for 24 hours is 0.4 day^{-1} (cross mark in Figure 1). Increasing the rescaling factors to 20% decreases the growth rate of the leading bred vector slightly presumably due to the nonlinear effects, while the spatial structure of the bred vector is almost identical to that for the rescaling factor of 3.3% (not shown).

On the other hand, when the rescaling factors are smaller than 1% of the climatological RMS χ_{200} variance, the growth rate increases enormously as the rescaling factor decreases. Previous studies pointed out that the fastest growing perturbations produced by the BGM method with considerably small rescaling factor are related to convective instability (Toth and Kalnay, 1997). Toth and Kalnay (1997) showed that perturbations associated

with the convective instability appear when the rescaling factor is set to be less than 1% of the climatological RMS variance of the 500-hPa stream function field. They also indicated that when the rescaling factor is reduced to less than 0.1% in the climatological RMS variance, the perturbation growth rate increases enormously. Therefore, it is plausible that the tropical bred vectors with the rescaling factors smaller than 1% are dominated by convective unstable modes. In fact, the tropical bred vectors less than 1% are dominated by an incoherent small-scale spatial structure, which is different from the situation for rescaling factors larger than 3.3% as we will see below. By choosing the appropriate variables, scaling amplitude, and scaling periods in the BGM method for the coupled general circulation model, Yang et al. (2006) also succeeded in isolating a slowly growing mode associated with the ENSO variability from baroclinic waves.

Figure 2 shows snapshots of χ_{200} and χ_{850} (850-hPa velocity potential) associated with $\mathbf{v}_1(t)$ on 26 November 2003 obtained using rescaling factors of 3.3% and 0.33%. With the rescaling factor of 3.3%, a pattern of planetary-scale structure in the upper-level divergence and convergence appears over the tropical Atlantic and the central Pacific regions, associated with dominant zonal wave number 1 (WN1) components (Figure 2a). This upper-level perturbation pattern accompanies lower-level convergence and divergence over those regions (Figure 2b), exhibiting a vertical baroclinic structure. Similar planetary-scale structure is also obtained for the tropical bred vectors produced with rescaling factors of 10%, 14.5% and 20% (not shown). On the contrary, a rescaling factor of 0.33% destroys coherent structure with the prevailing WN1 component in the tropics (Figures 2c and 2d). Instead, a small-scale horizontal structure becomes dominant particularly over the central Pacific for $\mathbf{v}_1(t)$, which also suggests the predominance of the convective unstable mode for extremely small rescaling factors.

Eastward phase propagation is another important feature of the leading tropical bred vector $\mathbf{v}_1(t)$. Figure 3 shows Hovmöller diagrams of χ_{200} averaged over the latitudinal band of 10°S-10°N for the observed field and for $\mathbf{v}_1(t)$ with the rescaling factors of 3.3% and 0.33%. The eastward propagation associated with the active phase of the observed tropical ISO becomes significant from December to early January (Figure 3a). In the following late January, the subsequent upper-level divergence and its eastward propagation associated with the tropical ISO are also observed over the Indian Ocean and the western Pacific. For the rescaling factor of 3.3%, eastward propagation with a phase speed of about 30 m s^{-1} (a period of about 15 days) dominated by WN1 components was frequently observed during this experimental period (Figure 3b). The eastward propagating bred vector slightly reduces its phase speed in December, but is still faster than the propagation of the tropical ISO. The eastward propagation of the bred vector begins over the Indian Ocean (30°E − 90°E), and becomes prominent over the western Pacific (90°E − 180°). In these regions, an eastward propagation of the tropical ISO is also most prominent (e.g., Hsu and Lee 2005). In late January when the next active phase of the tropical ISO initiates over the Indian Ocean, the eastward propagation of the bred vector tends to be fast, and WN2 and WN3 components develop particularly over the Indian Ocean. For the rescaling factor of 0.33%, on the other hand, no significant eastward propagation is observed, while a standing oscillation with small horizontal scale is dominant (Figure 3c). This fact also supports the predominance of the convective mode for the bred vector at 0.33% amplitude or smaller.

To further examine the eastward propagation characteristics of $\mathbf{v}_1(t)$, we performed space-time spectral analysis (Hayashi, 1982) for the χ_{200} perturbation averaged over the latitudinal band of 10°S-10°N for the rescaling factors of 3.3% and 0.33% (Figure 4). For the rescaling factor of 3.3%, the eastward propagating WN1 component with a frequency of 0.04-0.08 cycle per day (a period of 12.5-25 days) has a spectral peak (Figure 4a). Another weak spectral peak is also seen in the frequency of eastward propagating WN2 components. For the rescaling factor of 0.33% (Figure 4b), however, the spectral peak is obscure and high-frequency modes with small zonal structure attain relatively large amplitude, which implies the dominance of the convective mode.

It is interesting to note that the obtained tropical bred vector tapered in the extratropics has similar characteristics to the observed dry Kelvin waves in the tropics reported by previous studies (Milliff and Madden, 1996; Bantzer and Wallace, 1996). This similarity might be a key to understand the instability mechanism associated with the tropical ISO.

The tropical bred vectors with rescaling factors of 20% are operationally used in the monthly EPS since March

Table 1: Specifications of JMA medium-range EPS

	EPS0603 (Mar 2006 - Nov 2007)	EPS0711 (Nov 2007-)
EPS model	JMA-GSM TL159L40	JMA-GSM TL319L60
Generator of initial perturbations	BGM method	SV method
Perturbed area	20°S-90°N	20°S-90°N
Ensemble size	51	51
Forecast range	216 hours	216 hours

2007.

4 Medium-range EPS using initial perturbations with SVs

JMA has developed a medium-range EPS using a SV method for upgrade of the operational EPS. Concept of the simulation of initial condition uncertainties follows the same methodology developed at the European Centre for Medium-Range Weather Forecasts (ECMWF). Derived SVs are characterized by the maximum linear growth of total perturbation energy during a finite time interval.

In the JMA SV method, the model for calculating a forecast trajectory is a low resolution version of JMA-GSM, T63L40. SVs are computed using its linearised model (tangent-linear and adjoint models), which has been developed to operate the four-dimensional variational scheme on the current operational GDAS(Ohta and Okamoto, 2007), at the same resolution as the trajectory. The definition to measure perturbation growth is a widely used norm, namely total energy norm (Barkmeijer et al., 2001), as follows:

$$(\delta\mathbf{x},\delta\mathbf{x}) = \frac{1}{2}\int_D\int_1^{40}\left(u^2+v^2+\frac{c_p}{T_r}T^2\right)\left(\frac{\partial p}{\partial\eta}\right)d\eta dD + \frac{1}{2}R_dT_r\int_D\left(\frac{p_s}{p_r}\right)^2 dD + \varepsilon\frac{1}{2}\frac{L^2}{c_pT_r}\int_D\int_1^9 q^2\left(\frac{\partial p}{\partial\eta}\right)d\eta dD \tag{4}$$

where the terms u, v, T, p_s, and q are the perturbation $\delta\mathbf{x}$ of the zonal and meridional wind component, the temperature, surface pressure, and mixing ratio, respectively. T_r and p_r are the reference temperature (300K) and pressure (800hPa). Furthermore, c_p, R_d, and L indicate the specific heat at constant pressure, gas constant of dry air, and latent heat of condensation per unit mass, respectively. The integration extends over the interest horizontal domain D and vertical direction η of the model level over the surface ($1 \leq \eta \leq 40$). The integration range of moist energy term is limited from 1 to 9 (about 700hPa), not 40 (model top; 0.4hPa), in the model level for the below reason. The value of mixing ratio is quite small except the lower layer of the atmosphere although the atmosphere is high sensitive to change of mixing ratio.

In the moist energy term, ε is the weighting factor. Ehrendorfer et al. (1999) pointed out that for increasing ε, the contribution of the dry fields dominates initially, whereas the contribution of moisture dominates at the final time (vice versa for ε taken smaller). Our value of the parameter ε is small, 1/25, considering the larger uncertainty of initial fields on mixing ratio compared with other components.

Fifty perturbed analyses for the ensemble forecasting are generated by adding two types of initial condition perturbations to control analysis positively and negatively. The amplitude of (extra)tropical initial condition perturbations are set to be 26(12) % of the daily climatological 850 (500) hPa temperature variations such that the ensemble spread is similar to the error in short-range. Each perturbation's set is formed from linear combinations of targeted SVs (described in Table 2), $\delta\mathbf{x}^l (l = 1,2,\ldots,25)$, defined as follows:

Table 2: Two sets of targeted SVs for the medium-range EPS

	Extratropical SV	Tropical SV
Component	Initial 25 SVs and evolved 25 SVs	Initial 25 SVs and evolved 25 SVs
Resolution of SV calculation	T63L40	T63L40
Target area at initial and final times	30°N-90°N	20°S-30°N
Optimization time interval	48 hours	24 hours
Physics in linearised model	Simplified dry processes	Full processes

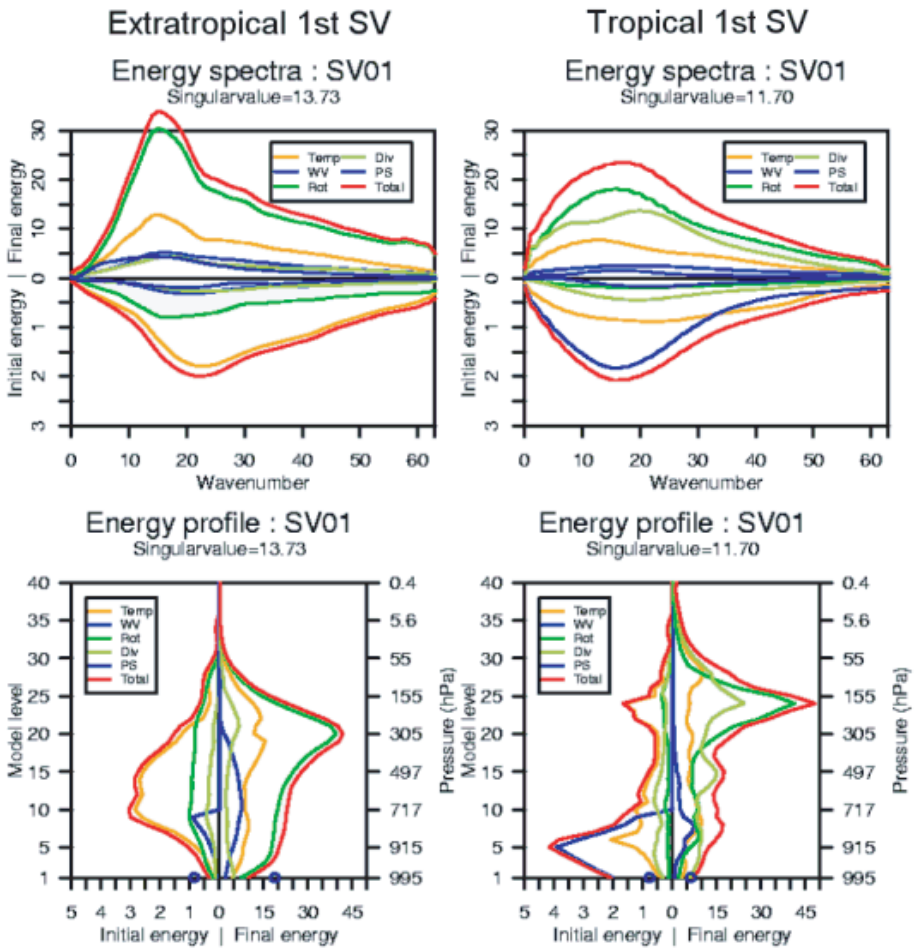

Figure 5: Spectral distributions (top panels) and vertical profiles (bottom panels) of contributions to total energy norm for the first extratropical (left panels) and tropical (right panels) SVs. Initial time is 12UTC on 2 August 2004. Energy at initial and final times are shown in bottom/ left and top/right sides of the same panel splitted with zero line, respectively. Individual panels consist of twelve (in case of spectra) or ten (in case of profile; the p_s contribution is plotted on the lowest level as circle.) curves. Orange, blue, green, light green, dark blue and red curves represent for the T, q, rotational, divergent, p_s, and all contributions, respectively.

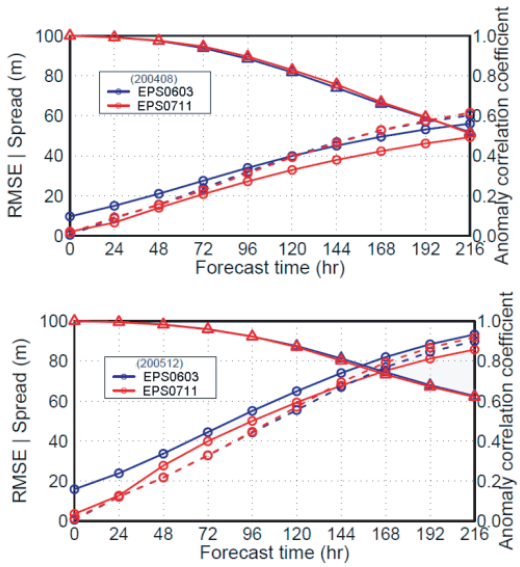

Figure 6: Monthly averaged time evolution of ACC(solid line with triangle marks) and RMSE(dashed line with circle marks) of ensemble mean forecast, and ensemble spread(solid line with circle marks). Red and blue colors are EPS0711 and EPS0603. Top and bottom panels show August 2004 and December 2005.

$$\mathbf{x}_e^l = \delta\mathbf{x}_e^l - \sum_{m=1}^{25} \left(\delta\mathbf{x}_e^l, \delta\mathbf{x}_i^m\right) \delta\mathbf{x}_i^m \tag{5}$$

$$\delta\mathbf{x}^l = \delta\mathbf{x}_i^l + \alpha \frac{\|\delta\mathbf{x}_i^l\|}{\|\mathbf{x}_e^l\|} \mathbf{x}_e^l \tag{6}$$

where the norm is the same definition defined in this section. $\delta\mathbf{x}_i^l$ is a growing perturbation linearly the optimization time (OT) ahead, namely initial SV. $\delta\mathbf{x}_e^l$ is a perturbation evolved linearly during the OT, namely evolved SV. Furthermore, l and α are the mode number of SV and the weighting factor on the evolved SV in creating initial condition perturbations, respectively. Not only unstable and small-scale perturbations but also stable and large-scale perturbations are included in an actual initial condition. And the small-scale and large-scale perturbations can be represented efficiently by initial SVs and evolved SVs, respectively.

The main differences between two sets of targeted SVs, tropical SVs and extratropical SVs, are spatial target area and the usage of the linearised model with full physical processes in the calculation. The full version of the linearised model is adopted to the calculation of tropical SVs because the processes in the tropics contribute significantly to perturbation growth (Barkmeijer et al., 2001). Our impact studies on inclusion of physical full processes in trial SV calculations (not shown) also supports the above work. And, to restrict the OT to 24 hours in the calculation of tropical SVs is effective in not only reducing the total computation time but also maintaining the linearity approximation in the tropics.

Figure 5 shows spectral distributions and vertical profiles of contributions to total energy norm for two first SVs. These panels are helpful to monitor the energy transfer and cascade. Panels about the extratropical SV illustrate the upscale energy propagation during 48 hours interval mainly from potential energy at the middle troposphere up to kinetic energy at the upper troposphere, indicating that the SV structure represents the typical baroclinic instability. On the other hand, panels about the tropical SV show the upward energy propagation during 24 hours interval mainly from moist energy at the lower troposphere up to kinetic energy at the upper troposhere. However, the upscale energy propagation is not remarkable relatively.

Figure 6 shows two scores of ensemble mean forecast and ensemble spread of geopotential heights at 500-hPa over the Northern Hemisphere (North of 20°N). The size of RMSEs and the anomaly correlation coefficients

Table 3: Specifications of Typhoon EPS

		Typhoon EPS
Resolution		60(km) × 60(km) with 60 layers
Initial time		00, 06, 12, 18UTC
Forecast range		132 hours (not fixed)
Number of targeted typhoons		3
Ensemble size		11
Perturbation	Generator	SV method
	Resolution	T63L40
	Area	RMSC: 100°E-180°, 20°N-60°N Typhoon: 20°× 10° (target)
	Physics in linearised model	RMSC: Simplified dry processes Typhoon: Full processes
	Optimization time	24 hours

(ACCs) between the new EPS (EPS0711) and the current EPS (EPS0603) are almost equal, indicating that deterministic products derived from EPS0711 are the same skill as that from EPS0603 in the medium-range. Although the overestimation of the EPS0603 spread in winter season are improved, the EPS0711 spread is underestimated to represent the size of the RMSE in the latter half of the forecast range in summer season.

5 Typhoon EPS using initial perturbations with SVs

The typhoon EPS (Table 3) uses the same SV method as the medium-range EPS, except for following points. The target areas are typhoon target area and mid-latitude Tokyo-typhoon center area (RMSC). Physics in the linearised model are the full processes for typhoon targeted SVs and simplified dry processes for the mid-latitude SVs. The weighting factor on the moist energy term ε is set to be 1. The typhoon EPS is semi-operational from May 2007, and will be operational in 2008. Typhoon intensity forecasting will be supported by 20km-GSM.

Figure 7 shows normalized energy vertical profiles for typhoon targeted SVs. The initial SV has a kinetic energy peak at the middle troposphere, while the final SV has a moist energy peak at the lower troposphere and kinetic energy peak at the upper and middle troposphere. Figure 8 shows vertically accumulated total energy fields of the 5 leading SVs targeted for typhoon. The initial SVs have large structures surrounding the typhoon, while the final SVs are confined near the center.

6 Conclusion

The tropical bred vectors are derived from a modified breeding cycle in which the perturbations are damped over the extratropics beyond 20° and their norm is defined by the RMS variance of 200-hPa velocity potential (χ_{200}) in the tropics. When the prescribed magnitude of the norm is greater than 3.3% of the climatological RMS χ_{200} variance, at least two growing bred vectors with time-averaged growth rate of 0.1 day^{-1} are obtained. The growth rate of the tropical bred vectors is smaller than that of the baroclinic instability in the extratropics, but is clearly differentiated from the small-scale convective instability that dominates perturbation for extremely small magnitude of the norm. These tropical bred vectors are characterized by eastward propagating zonal wave number 1 components of the first baroclinic structure with a phase speed of about 30 m s^{-1}.

It is also interesting to note that those growing bred vectors have similar space-time characteristics with east-

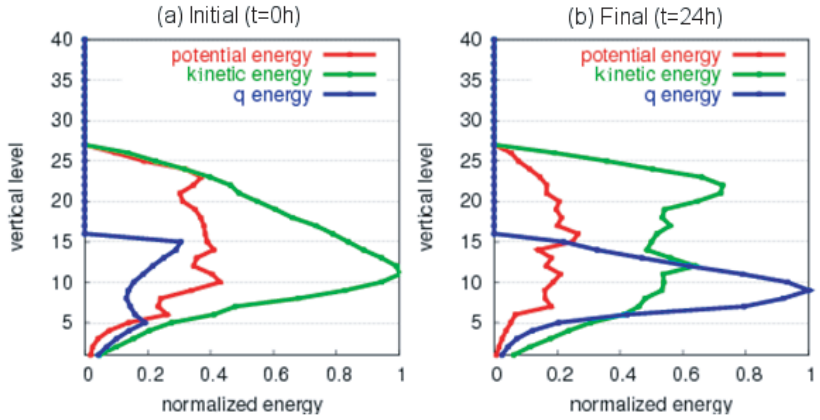

Figure 7: Average initial-time(left) and final-time(right) energy vertical cross section. The averages have been computed considering the leading 5 SVs from 5 August 2005 to 24 september 2005.

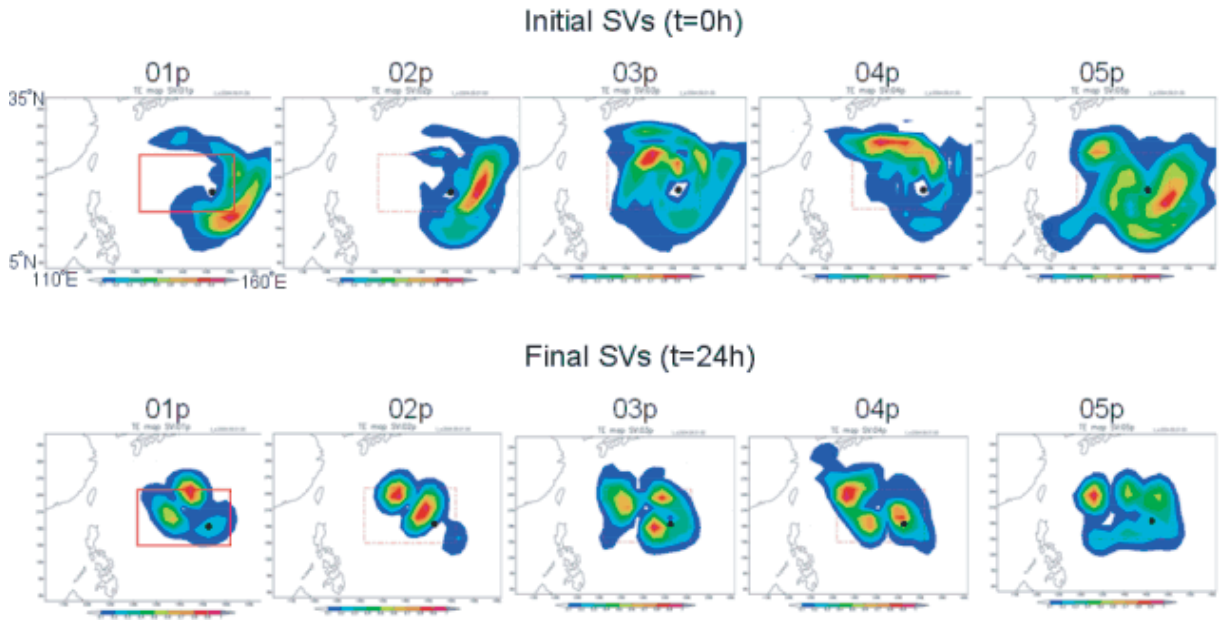

Figure 8: Vertically accumulated total energy fields of the five leading SVs targeted for typhoon at 00UTC 01 September 2004. The initial typhoon location is indicated by a black dot. The typhoon target area is indicated by a red rectangle.

ward propagating dry Kelvin waves detected by observational analysis (Milliff and Madden, 1996; Bantzer and Wallace, 1996). This similarity might be a key to understand the instability mechanism associated with the tropical ISO. We are now conducting further analysis to reveal the instability mechanism of the tropical ISO and the dependence of the predictability of the tropical ISO on its phase and activity using the bred vectors developed in this study.

We have developed a new medium-range EPS (typhoon EPS) using a SV method. The simulation of the perturbation is similar to one at ECMWF. Our method is characterized by using two sets of targeted SVs, over the extratropical Northern Hemisphere and the whole tropics for the medium-range EPS (mid-latitude RMSC area and typhoon area for the typhoon EPS), that are the component of extratropical and tropical perturbations, respectively. The structure of the extratropical perturbations is characteristic of baroclinic mode. On the other hand, the tropical perturbations for the medium-range EPS (typhoon EPS) are generated to grow up in response to initial moist fields (kinetic fields). Regarding the tropical perturbations, the energy propagation is controled to set a certain weight on the moist energy term of the norm definition. Although our perturbations are considered unstable structures during the finite time, our trial SV calculation suggests the dependency of spectral distribution on the optimization time interval. Further study is necessary to research the effective way of SV calculation for tropical ensemble forecasting.

References

Bantzer, C. H., and J. M. Wallace, 1996: Intraseasonal variability in tropical mean temperature and precipitation and their relation to the tropical 40-50 day oscillation. *J. Atmos. Sci.*, **53**, 3032-3045.

Barkmeijer, J., R. Buizza, T. N. Palmer, K. Puri, and J.-F. Mahfouf, 2001: Tropical singular vectors computed with linearized diabatic physics. *Q. J. R. Meteorol. Soc.*, **127**, 685-708.

Chikamoto, Y., H. Mukougawa, T. Kubota, H. Sato, A. Ito, and S. Maeda, 2007: Evidence of growing bred vector associated with the tropical intraseasonal oscillation. *Geophys. Res. Lett.*, **34**, L04806, doi:10.1029/2006GL028450.

Ehrendorfer, M., R. M. Errico, and K. D. Raeder, 1999: Singular-vector perturbation growth in a primitive equation model with moist physics. *J. Atmos. Sci.*, **56**, 1627-1648.

Hayashi, Y., 1982: Space-time spectral analysis and its applications to atmospheric waves. *J. Meteorol. Soc. Jpn.*, **60**, 156-171.

Hsu, H.-H., and M.-Y. Lee, 2005: Topographic effects on the eastward propagation and initiation of the Madden-Julian Oscillation. *J. Clim.*, **18**, 795-809.

Jones, C., D. E. Waliser, K. M. Lau, and W. Stern, 2004: The Madden-Julian Oscillation and its impact on Northern Hemisphere weather predictability. *Mon. Weather Rev.*, **132**, 1462-1471.

Kubota, T., H. Mukougawa, and T. Iwashima, 2005: Predictability of Madden and Julian oscillation in JMA one-month forecasts. *Ann. Disaster Prev. Res. Inst. Kyoto Univ.*, **48B**, 475-490.

Madden, R. A., and P. R. Julian, 1994: Observation of the 40-50 day tropical oscillation: A review. *Mon. Weather Rev.*, **122**, 814-837.

Milliff, R. F., and R. A. Madden, 1996: The existence and vertical structure of fast, eastward-moving disturbances in the equatorial troposphere. *J. Atmos. Sci.*, **53**, 586-597.

Ohta, Y., and K. Okamoto, 2007: Global analysis. Outline of the Operational Numerical Weather Prediction at the Japan Meteorological Agency. *JMA*, 18-28.

Toth, Z., and E. Kalnay, 1993: Ensemble forecasting at NMC: The generation of perturbations. *Bull. Am. Meteorol. Soc.*, **74**, 2317-2330.

Toth, Z., and E. Kalnay, 1997: Ensemble forecasting at NCEP and the breeding method. *Mon. Weather Rev.*, **125**, 3297-3319.

Waliser, D. E., K. M. Lau, W. Stern, and C. Jones, 2003: Potential predictability of the Madden-Julian Oscillation. *Bull. Am. Meteorol. Soc.*, **84**, 33-50.

Yang, S.-C., M. Cai, E. Kalnay, M. Rienecker, G. Yuan, and Z. Toth, 2006: ENSO bred vectors in coupled ocean-atmosphere general circulation models. *J. Clim.*, **19** 1422-1436.